ISSN 0001-4338, Izvestiya, Atmospheric and Oceanic Physics, 2019, Vol. 55, No. 1, pp. 86–98. © Pleiades Publishing, Ltd., 2019.
Russian Text © A.R. Jakovlev, S.P. Smyshlyaev, 2019, published in Izvestiya Rossiiskoi Akademii Nauk, Fizika Atmosfery i Okeana, 2019, Vol. 55, No. 1.

Impact of the Southern Oscillation on Arctic Stratospheric Dynamics and Ozone Layer

A. R. Jakovlev[a], * and S. P. Smyshlyaev[a]

[a] *Russian State Hydrometeorological University, St. Petersbourg, 192007 Russia*

**e-mail: endrusj@rambler.ru*

Received July 16, 2018; revised September 28, 2018; accepted November 28, 2018

Abstract—The impact of the Southern Oscillation on the structure and composition of the Arctic stratosphere is analyzed using sea-surface temperature, potential vorticity, air temperature, ozone mixing ratio, and total ozone reanalysis data for 1980–2016. It is shown that El Niño enhances the instability of the stratospheric circumpolar vortex and precedes sudden stratospheric warmings, thus leading to an increase in total ozone over the Artcic during winter–spring.

Keywords: El Niño, La Niña, sudden stratospheric warming, stratospheric circumpolar vortex, ozone hole

DOI: 10.1134/S0001433819010122

INTRODUCTION

The ocean–atmosphere interaction influences atmospheric physical and chemical processes. These processes determine the exchange of properties and energy conversion. The Sun, which heats the upper layer of the ocean, thus inducing temperature and density gradients and, consequently, ocean currents, is a major source of energy for them [1–3].

The most important is an eastern tropical Pacific current which warms the ocean surface and is related to El Niño. The opposite phase of El Niño is La Niña, cooling the ocean surface. The atmospheric component tied to El Niño is the Southern Oscillation. It is an oscillation in surface air pressure between the eastern and western Pacific Ocean waters, which leads to deep convection and high moistening [4].

The ocean–atmosphere interaction is a subject of numerous scientific studies [1, 2, 5–7] in which various models have been developed for the analysis and prediction of the processes linked to this event. The oceanic impact on the stratosphere and polar regions has become an urgent problem over the last few years [8–10].

One important dynamic process occurring in the polar stratosphere is the circumpolar vortex, which has a strong influence on the polar stratospheric temperature and composition. The stability of the circumpolar vortex depends on the stability of the zonal flow, while the meridional flow causes its instability [11]. Numerical experiments have shown that average zonal winds are weaker in the Arctic than in the Antarctic, while interannual variations, on the contrary, are larger in the Arctic than in the Antarctic [12]. A change in conditions at the lower boundary of the stratosphere is sufficient for a distinction in the time variability of the mean flow around the pole. Planetary waves are one of the key factors in the existence of the circumpolar vortex in the Northern Hemisphere. The vortex stability also influences the amount of ozone and temperature: theoretically, the longer the circumpolar vortex exists, the longer the ozone hole will persist and the lower the polar stratospheric temperature will be [13].

The temperature of the polar lower stratosphere is the key factor in changing the magnitude of ozone loss. The cold winter season of 1996–1997, which resulted from weak wave activity, led to the enhancement of ozone destruction by heterogeneously activated chlorine and bromine compounds and to a weakening of planetary waves. The warm winter season of 1998–1999, on the contrary, was driven by high wave activity [12]. The temperature inside the polar stratospheric vortex determines the volume of polar stratospheric clouds, which the rate of ozone destruction depends upon. The weaker planetary waves can lead to a decrease in polar stratospheric temperatures and to less transport of ozone, resulting in a warmer tropical tropopause [12, 14].

Sea-surface temperature (SST) variations, producing a meridional SST gradient, can have a significant influence on the stratosphere [13]. The meridional SST gradient influences zonal circulation more considerably than global SST variability. Hence, the SST gradient has a strong influence on the circumpolar vortex and ozone in the Northern Hemisphere. It has also been hypothesized that ozone decline can influence the El Niño–Southern Oscillation, which redistributes heat fluxes in the ocean and atmosphere,

while ozone enhancement can favor La Niña events [15]. This can lead to a transport of the ozone-absorbed ultraviolet radiation energy into the ocean, thus increasing its heat capacity. Numerical modeling has shown that the influence of El Niño on the European surface climate occurs via a stratospheric pathway [28].

The aim of this paper is to investigate the influence of sea-surface temperature on Arctic stratospheric processes (the circumpolar vortex, temperature changes, and ozone changes). For this, periods from December through March were considered for the most illustrative years: 1996–1997, 1998–1999, 2009–2010, 2010–2011, 2014–2015, and 2015–2016.

Section 1 describes initial data and methodology. Section 2 presents the results. The conclusions follow in Section 3.

1. INITIAL DATA AND METHODOLOGY

The data used in this study are the air temperature, ozone mixing ratio, and potential vorticity from the Modern-Era Retrospective analysis for Research and Application (MERRA), the European Centre for Medium-Range Weather Forecasts (ECMWF) interim ReAnalysis (ERA-Interim), the ECMWF Twentieth Century ReAnalysis (ERA-20C), and ERA5 [16, 17]. There are 25 vertical levels in MERRA and 21 levels in ERA-Interim, ERA-20C, and ERA5. Total column ozone data from these reanalyses were also used. To examine the oceanic impact on the atmosphere, SST data from Met Office [18], ERA-Interim [17], ERA-20C prior to 2010, and ERA5 for 2010–2015 [17] were used.

For data analysis, a period was chosen to be from 1980 through 2016, with monthly means being used. Daily means of potential vorticity, air temperature, and ozone mixing ratio were also used for 1997, 1999, 2010, 2011, 2015, and 2016.

The reanalysis data were reduced to a grid of the chemistry–climate model developed at the Institute of Numerical Mathematics, Russian Academy of Sciences [19], and at the Russian State Hydrometeorological University [20], which was used in the previous research [21]. The resolution of the grid is $4° \times 5°$; the model domain extends from 180° W to 180° E in longitude, from 88° S to 88° N in latitude, and from the surface to 0.003 hPa (from 0 to 88 km) in the vertical (with 39 σ levels).

To analyze stratospheric processes, the following projections and profiles were constructed:

Polar projections of potential vorticity on a surface with a potential temperature of 550 K;

Polar projections of air temperature and ozone mixing ratio at 24.5 km (30 hPa) in the Northern Hemisphere;

Polar projections of total ozone in the Northern Hemisphere;

Polar projections of SST anomalies;

Vertical profiles of the annual variations in potential vorticity; air temperature; and ozone mixing ratio in 1997, 1999, 2010, 2011, 2015, and 2016 at 84° N.

2. RESULTS

2.1. Analysis of Oceanic Processes

The distribution of SST anomalies from the ERA-Interim monthly means is shown in Fig. 1. The years were chosen in which the influence of El Niño and La Niña was most significant: 1996–1997 and 1998–1999 (rows (a), (b)), because one of the severest El Niño events occurred in 1997–1998 [22]. The figure also shows 2009–2010 (row (c); El Niño year), 2010–2011 (row d); La Niña year), and 2014–2015 and 2015–2016 (rows (e), (f); El Niño years). The SST anomalies are plotted for December–January (column (1)) and February–March (column (2)).

A strong warming is seen in the tropical Pacific in El Niño years (2010, 2015, and 2016; rows (c), (e), (f)). Signs of warming are also evident in February–March 1997 (Fig. 1a–(2)). The SST anomalies in this region were above 1 K, which indicates that SST exceeded 300 K (27°C). The region of the largest SST anomalies (above 2–3 K) is in the south Pacific. In El Niño years (2010, 2015, and 2016), this region extends northward beyond the equator and SST anomalies are greater than 3 K. The warming is most pronounced in 2015 and 2016 (there was a region of high SST anomalies in the equatorial Pacific in these years). In 2009–2010 from December through March, the warm Pacific region shifts to the east toward the western American coast, an indicator of the El Niño event. This region persists continuously from December 2015 through March 2016, which suggests that the El Niño in this period was fairly strong. From December through March 2014–2015, the development of El Niño is more prominent than in 2009–2010. A region of low SST anomalies (less than −1 K) exists in the equatorial Pacific from December through March 1998–1999 (row (b)) and 2010–2011 (row (d)). This indicates that El Niño in these years was succeeded by an opposite phase, La Niña, which resulted in a cooling of the eastern tropical Pacific. An analysis of the Met Office, ERA-20C, and ERA5 SSTs yields similar results.

Thus, it can be concluded that El Niño events occurred in 1997, 2010, 2015, and 2016, while 1999 and 2011 were the La Niña years.

2.2. Circumpolar Vortex and Oceanic Impact

The stratospheric circumpolar vortex (CPV) is an area in the altitude range from the lower stratosphere to the mesosphere with severe westerlies, having a maximum around 60° N, and low pressures. According to [11–14], a stable CPV decreases stratospheric temperatures and reduces the ozone concentration. In

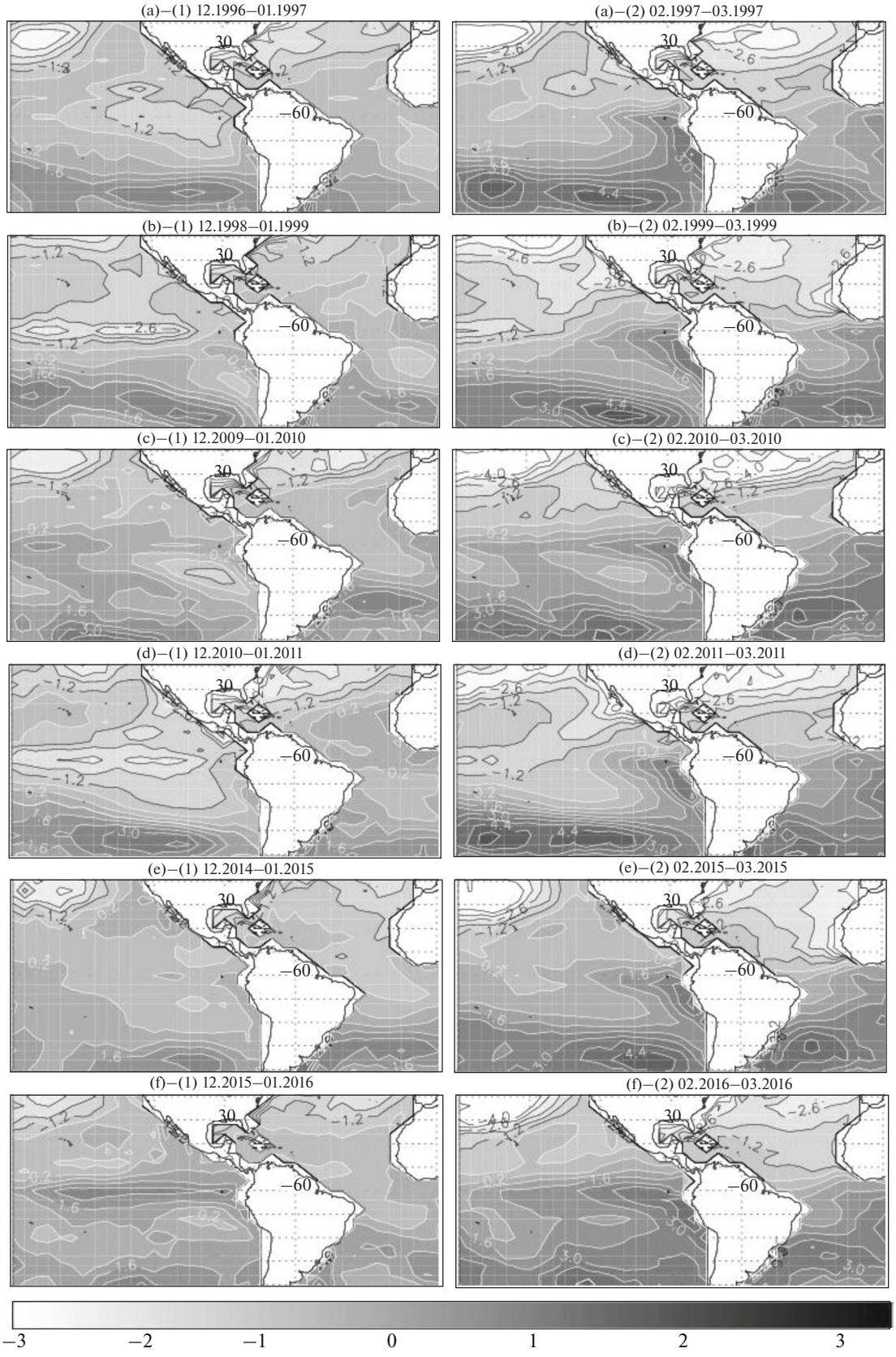

Fig. 1. Distribution of the 2-month mean anomalies in sea surface temperature (in K) in the 40° S–40° N, 180° W–0° region from ERA-Interim for (column (1)) December–January and (column (2)) February–March in (row (a)) 1996–1997, (row (b)) 1998–1999, (row (c)) 2009–2010, (row (d)) 2010–2011, (row (e)) 2014–2015, and (row (f)) 2015–2016.

late winter, a stable CPV leads to the more intense destruction of ozone. In El Niño years, more wave activity propagates from the troposphere to the polar stratosphere, weakening the CPV [29].

Figure 2 shows polar projections of potential vorticity (PV) on the 550 K isentropic surface in the Northern Hemisphere from the ERA-Interim monthly means. The years were chosen to be the same as those for SST: 1996–1997 and 1998–1999 (rows (a), (b)), 2009–2010 and 2010–2011 (rows (c), (d)), and 2014–2015 and 2015–2016 (rows (e), (f)). The PV projections are given for the following months: December and February 1996–1997; January and February 2010; and February and March 1999, 2011, 2015, and 2016.

It can be seen that the CPV is most stable in 1997, 2011, and 2015 (rows (a), (d), (e)). In 1997 and 2011, the CPV develops from December to February: the values of PV over the Arctic increase from $0.4–0.6 \times 10^{-4} \frac{\mathrm{K\,m^2}}{\mathrm{kg\,s}}$ to more than $1.3–1.5*10^{-4} \frac{\mathrm{K\,m^2}}{\mathrm{kg\,s}}$, while PV in March ($1.5 \times 10^{-4} \frac{\mathrm{K\,m^2}}{\mathrm{kg\,s}}$) is close to its February value. In 2015, the CPV is also stable, but PV does not exceed $1.0 \times 10^{-4} \frac{\mathrm{K\,m^2}}{\mathrm{kg\,s}}$. In 1999 (row (b)), the CPV is most unstable: although the PV value over the Arctic in December 1998 was about $1.0 \times 10^{-4} \frac{\mathrm{K\,m^2}}{\mathrm{kg\,s}}$, it decreased to $0.5 \times 10^{-4} \frac{\mathrm{K\,m^2}}{\mathrm{kg\,s}}$ in January and then it increased again to $0.9 \times 10^{-4} \frac{\mathrm{K\,m^2}}{\mathrm{kg\,s}}$ in February (Fig. 2b–(1)), after which the CPV almost decayed in March (Fig. 2b–(2)). In 2010 and 2016 (rows (c), (f)), the CPV developed from December to January (with PV values of up to $1.0 \times 10^{-4} \frac{\mathrm{K\,m^2}}{\mathrm{kg\,s}}$), but began to break down in March.

We also constructed vertical zonal-mean annual PV profiles from the ERA-Interim daily means, which are shown in Fig. 3. Profiles for 1997, 1999, 2010, 2011, 2015, and 2016 at 84° N are plotted in Figs. 3a–3f.

As can be seen from these figures, the CPV exists during the period when PV values show large fluctuations, while there is no CPV when fluctuations are small. The most stable CPV was in 1997 (Fig. 3a), existing from January to April in this year. Stable CPVs were typical of 2011 (Fig. 3d) and 2015 (Fig. 3e), but they lasted until the latter half of March. In 2010 (Fig. 3c) and 2016 (Fig. 3f), the CPV was also decaying during March. In 1999 (Fig. 3b), the CPV existed only until mid-February, which indicates that it was unstable. For 60° N, where St. Petersburg lies, the reanalysis data give similar results.

The results were similar in MERRA, ERA-20C, and ERA5 data.

Thus, it can be concluded that the most stable CPVs occurred in the years before the onset of a severe El Niño, in 1997 and 2015, and also in 2011, a La Niña year. In 1999, when the La Niña began after the severe 1997–98 El Niño, the CPV was most unstable. In a weak El Niño year (2010) and the year of a mature El Niño (2016), the CPV was fairly stable, but began to break down in March. This suggests that the stability of the CPV can be an indication of the onset of El Niño, while instability can be a consequence of it.

2.3. Stratospheric Temperature and Oceanic Impact

The stratospheric temperature depends on the CPV stability; it influences the atmospheric composition and, hence, ozone [12, 23].

Polar projections of air temperature at 24.5 km (30 hPa) over the Northern Hemisphere from the ERA-Interim monthly means are shown in Fig. 4. The years were taken to be the same as those for SST and PV: 1996–1997 and 1998–1999 (columns (a), (b)), 2009–2010 and 2010–2011 (columns (c), (d)), and 2014–2015 and 2015–2016 (columns (e), (f)). The projections of air temperature are given for the following months: January and February 2010, January and March 2016; December and January 2014–2015; and February and March 1997, 1999, and 2011.

As can be seen, the polar region of low temperatures with values below 200 K was most stable in 1997 and 2011 (columns (a), (d)), which corresponds to the most stable CPV in these years (see Fig. 2, columns (a), (d)). The low-temperature region in these years is the largest from December through February (temperatures below 200 K over the Arctic Ocean) and then decreases and remains only over the North Pole. In 2015, the low-temperature region is less stable: although the zone with temperatures below 200 K was large in December 2014 (Fig. 4e–(1)), it disappeared almost entirely in January 2015 (Fig. 4e–(2)), but reemerged in February. In 2010 and 2016 (columns (c), (f)), low-temperature regions with values below 200 K existed only in December and January, after which they disappeared (warm zones with temperatures above 230 K appeared in their place). In 1999 (the most unstable CPV; column (b)), there was a fairly stable low-temperature region with values of 205–210 K, although it dissipated in March (Fig. 4b–(2)).

Vertical zonal-mean annual air-temperature profiles were also constructed from the ERA-Interim daily means; they are shown in Fig. 5. The profiles for 1997, 1999, 2010, 2011, 2015, and 2016 at 84° N are plotted in Figs. 5a–5f.

Cool temperatures (below 200 K) persist in the lower stratosphere (up to 35 km) from January to

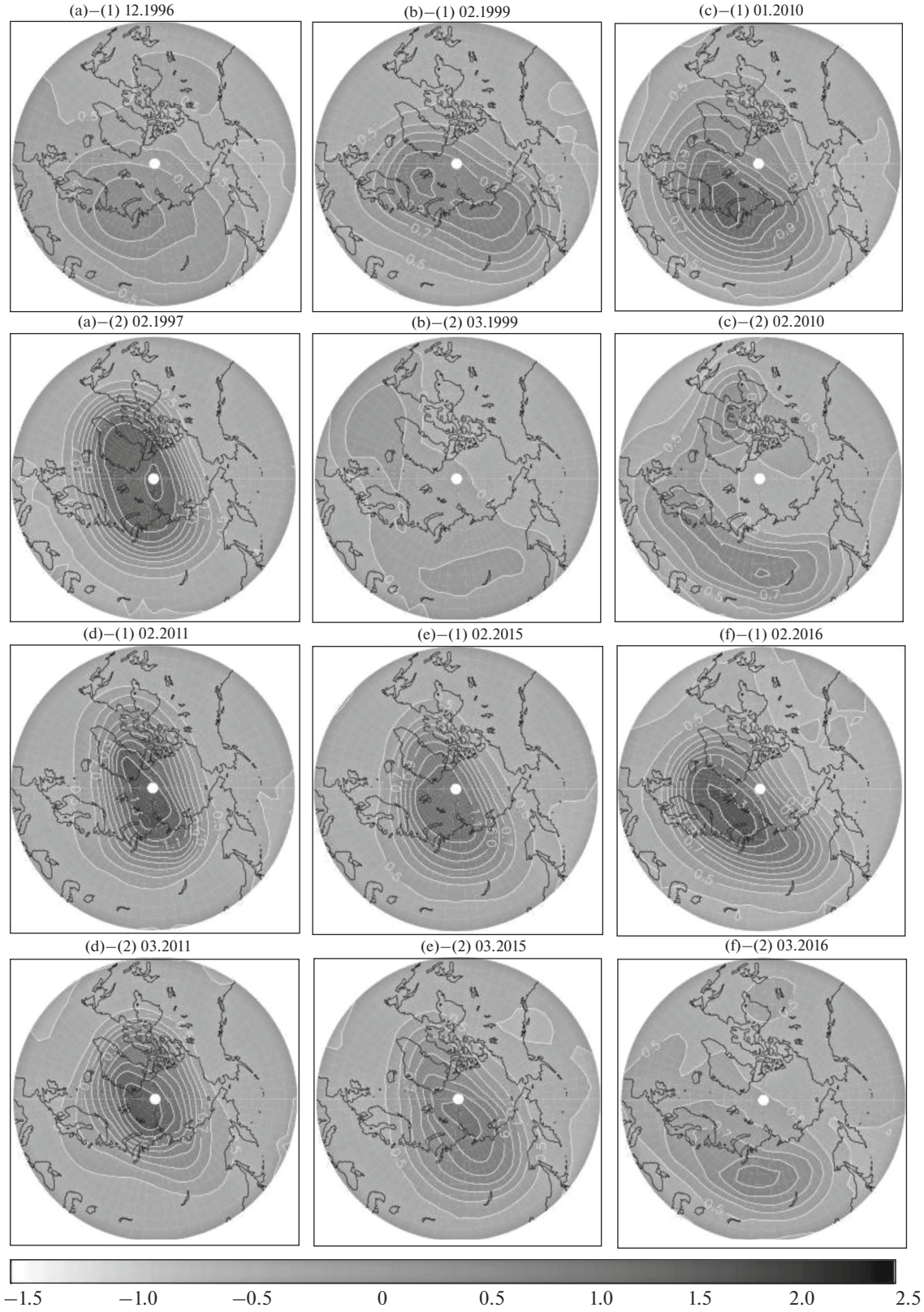

Fig. 2. Monthly mean distribution of potential vorticity (in $10^4 \frac{\text{K m}^2}{\text{kg s}}$) over the Northern Hemisphere in the 40° N–90° N region at 24.5 km (30 hPa) from ERA-Interim for (column (a)) December and February 1996–1997, (column (b)) February and March 1999, (column (c)) January and February 2010, (column (d)) February and March 2011, (row (e)) 2015, and (row (f)) 2016.

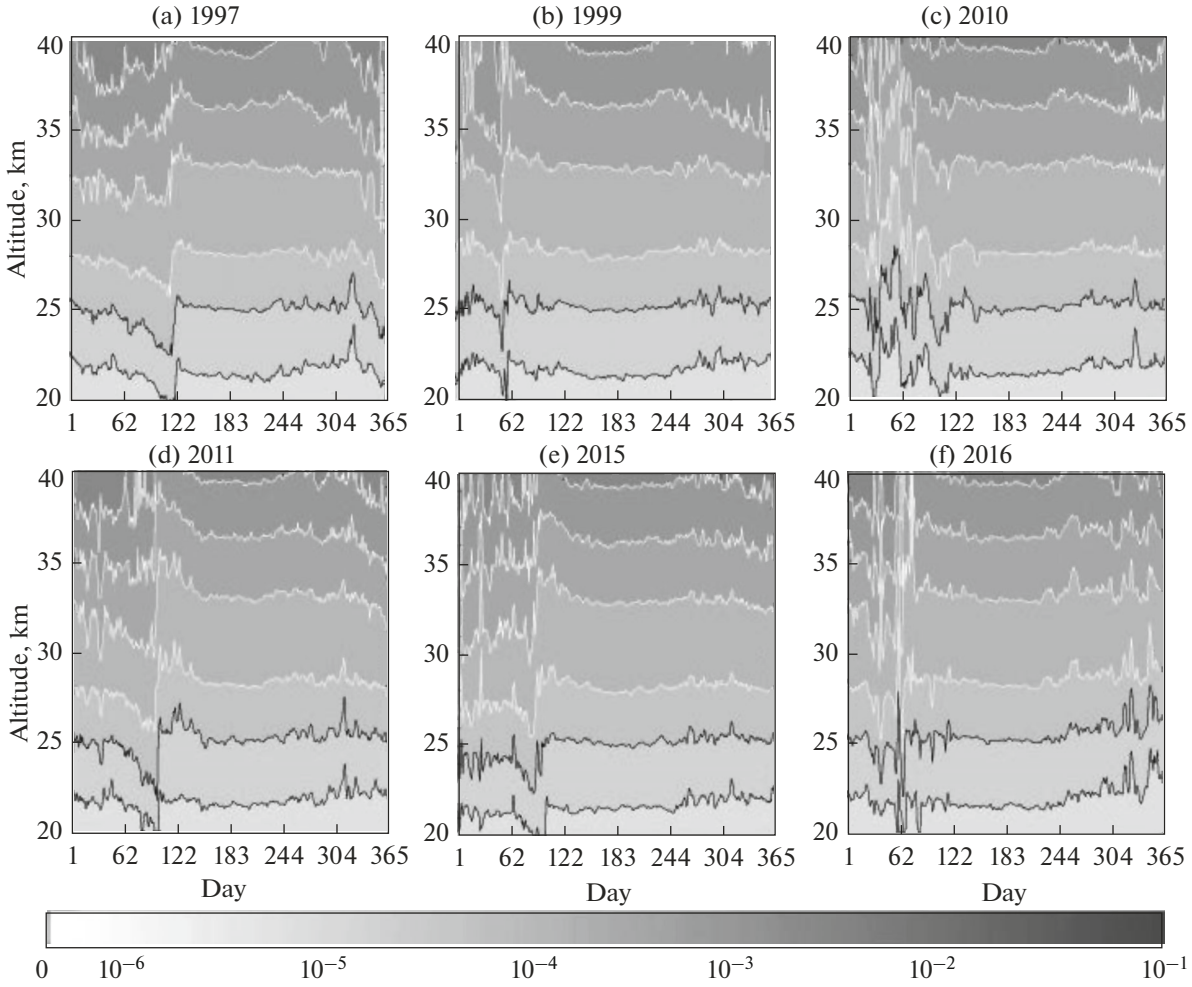

Fig. 3. Vertical annual profiles of potential vorticity (in $\frac{\text{K m}^2}{\text{kg s}}$) at 84° N from ERA-Interim daily means in (a) 1997, (b) 1999, (c) 2010, (d) 2011, (e) 2015, and (f) 2016.

March and from October to December. Warm temperatures (above 260 K) occur at altitudes above 30 km from May to September, which is consistent with the seasonal cycle. However, low-temperature periods are disrupted by sudden stratospheric warmings (SSWs), in which the stratospheric temperature rises by several tens of degrees above normal [23, 24]. In the Northern Hemisphere, SSWs occur nearly every winter because of wave activity [24–26]. These SSWs may be forced by El Niño or by the quasi-biennial oscillation of zonal wind [23–26] and are able to influence the stability of the CPV. An examination of 53 years of reanalysis data with major SSWs, affecting the tropospheric circulation, has shown that they occur with nearly equal probability during warm and cold phases of the El Niño–Southern Oscillation [30].

According to Fig. 5, SSWs are almost missing at polar latitudes in 1997 (Fig. 5a) and 2011 (Fig. 5d): a stable cold zone with temperatures below 200 K exists from January to April. At that time, SSWs were frequent at 60° N but had no influence on the CPV stability because they developed outside the polar region. The SSWs were most often observed at polar latitudes from January through April 2010 (Fig. 5c) and 2015 (Fig. 5e), when the temperature periodically rose to 230 K. These SSWs led to the instability of the cold region over the North Pole in those years. There was a low-temperature region at polar latitudes from January to March 2016 (Fig. 5f), after which came a series of SSWs. A similar situation was in 1999 (Fig. 5b).

The analysis of MERRA, ERA-20C, and ERA5 yields analogous results for air temperature and SSWs.

Thus, the CPV and the low-temperature region related to it were most stable in 1997 and 2011. With a stable CPV in 2015, the series of SSWs resulted in the instability of the low-temperature region, and the CPV also lost stability. In 1999, when the CPV was most unstable, the situation with SSWs was close to

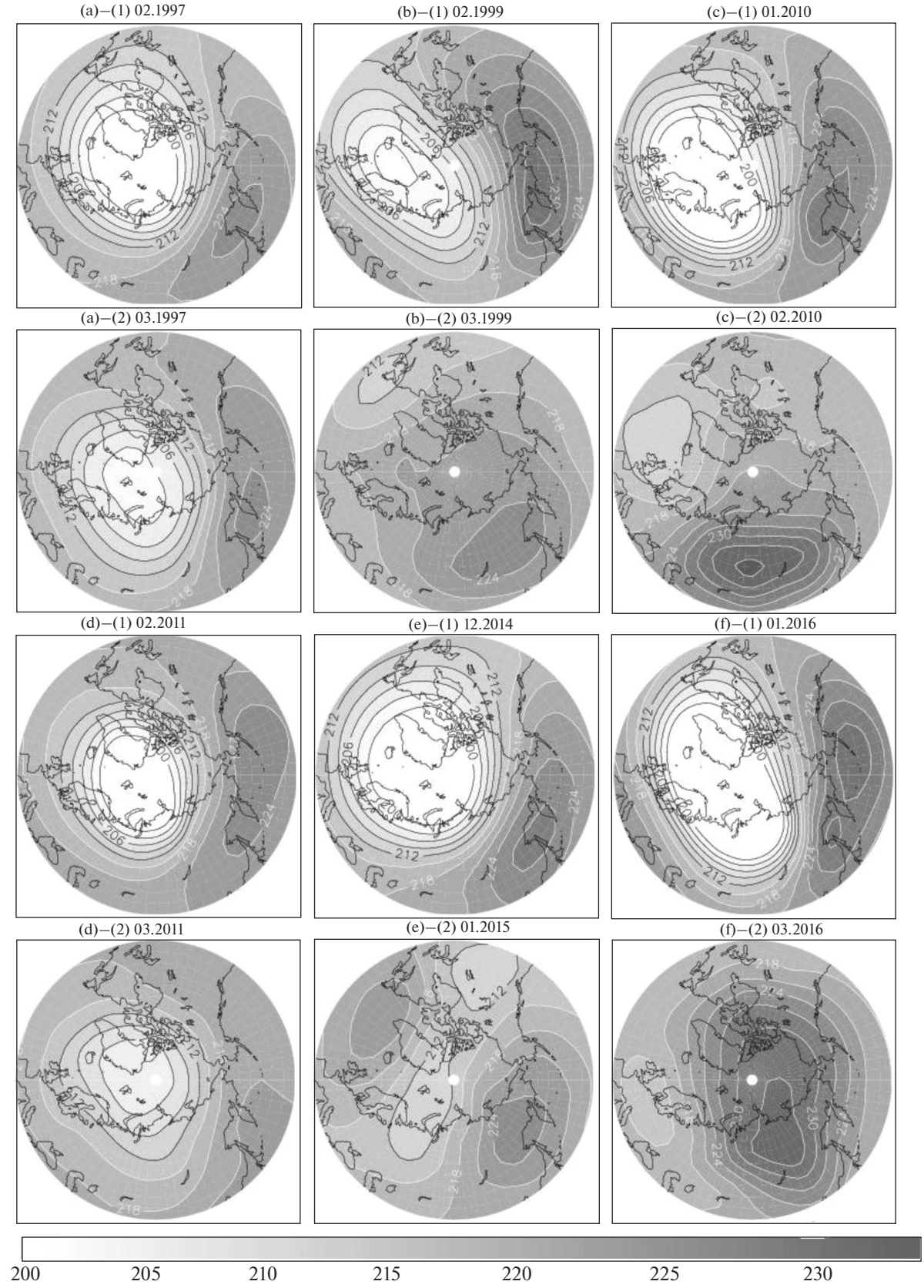

Fig. 4. Monthly mean distribution of air temperature (in K) over the Northern Hemisphere in the 40° N–90° N region at 24.5 km (30 hPa) from ERA-Interim for February and March (column (a)) 1997 and (column (b)) 1999, (column (c)) January and February 2010, (column (d)) February and March 2011, (column (e)) December and January 2014–2015, and (column (f)) January and March 2016.

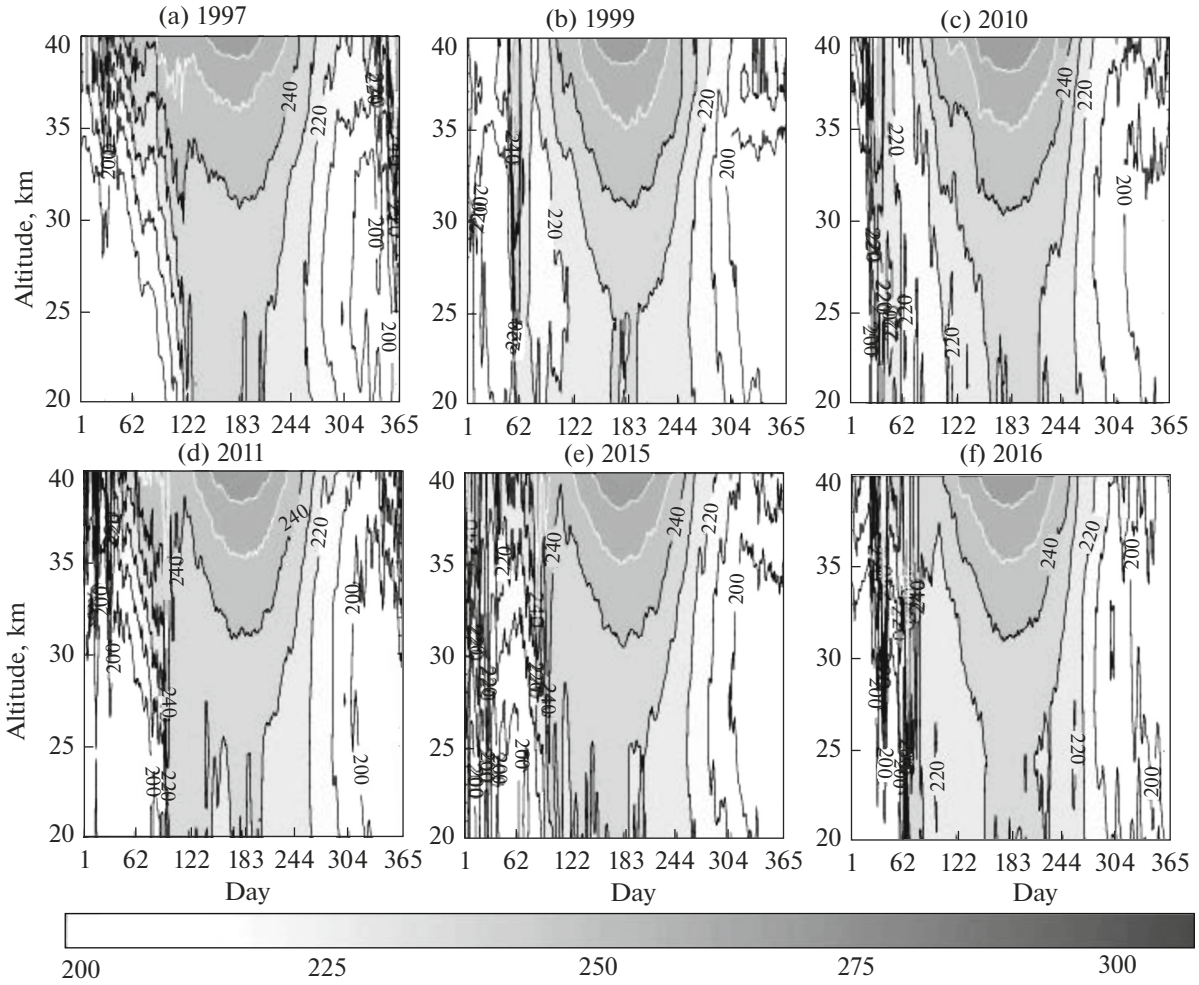

Fig. 5. Vertical annual profiles of air temperature (in K) at 84° N from the ERA-Interim daily means in (a) 1997, (b) 1999, (c) 2010, (d) 2011, (e) 2015, and (f) 2016.

that observed in 2016. Hence, SSWs can be a consequence of El Niño, while the lack of SSWs can indicate the occurrence of La Niña or no Southern Oscillation in those years.

2.4. Ozone Layer and Oceanic Impact

The state of the ozone layer depends on a variety of factors, but a key one is the stability of the CPV and the cold core, particularly over the polar region. A stable CPV results in a stable low-temperature polar zone, which, in turn, may cause the appearance of polar stratospheric clouds; the activation of heterogeneous processes on their surface; and, hence, a reduction in the ozone concentration [12, 15, 26, 27].

Polar projections of the ozone mixing ratio at 24.5 km (30 hPa) over the Northern Hemisphere from the ERA-Interim monthly means are shown in Fig. 6. The years are the same as those for other data: 1996–1997 and 1998–1999 (columns (a), (b)), 2009–2010 and 2010–2011 (columns (c), (d)), and 2014–2015 and 2015–2016 (columns (e), (f)). Projections of the ozone mixing ratio are given for January and February 1997 and 2010, December and January 1998–1999, February and March 2011, December and February 2014–2015, and January and March 2016.

As can be seen in the figure, in 1997 (column (a)) over the North Pole, there was a stable zone of the low ozone mixing ratio (far below the long-term means) with values of $4 \times 10^{-6} \frac{\text{kg}}{\text{kg}}$ (2.4 ppm), which matches a stable CPV and a low-temperature region, although this value increased to $7 \times 10^{-6} \frac{\text{kg}}{\text{kg}}$ (4.2 ppm) in March. There was a less distinct ozone decline ($6–7 \times 10^{-6} \frac{\text{kg}}{\text{kg}}$, or 3.6–4.2 ppm) in 2011 (column (d); this year was also noteworthy for a stable CPV and a stable low-temperature region), with a significant ozone decline beginning in March, which was caused by chemical processes [11]. In 2010 (column (c)), 2015 (column (e)),

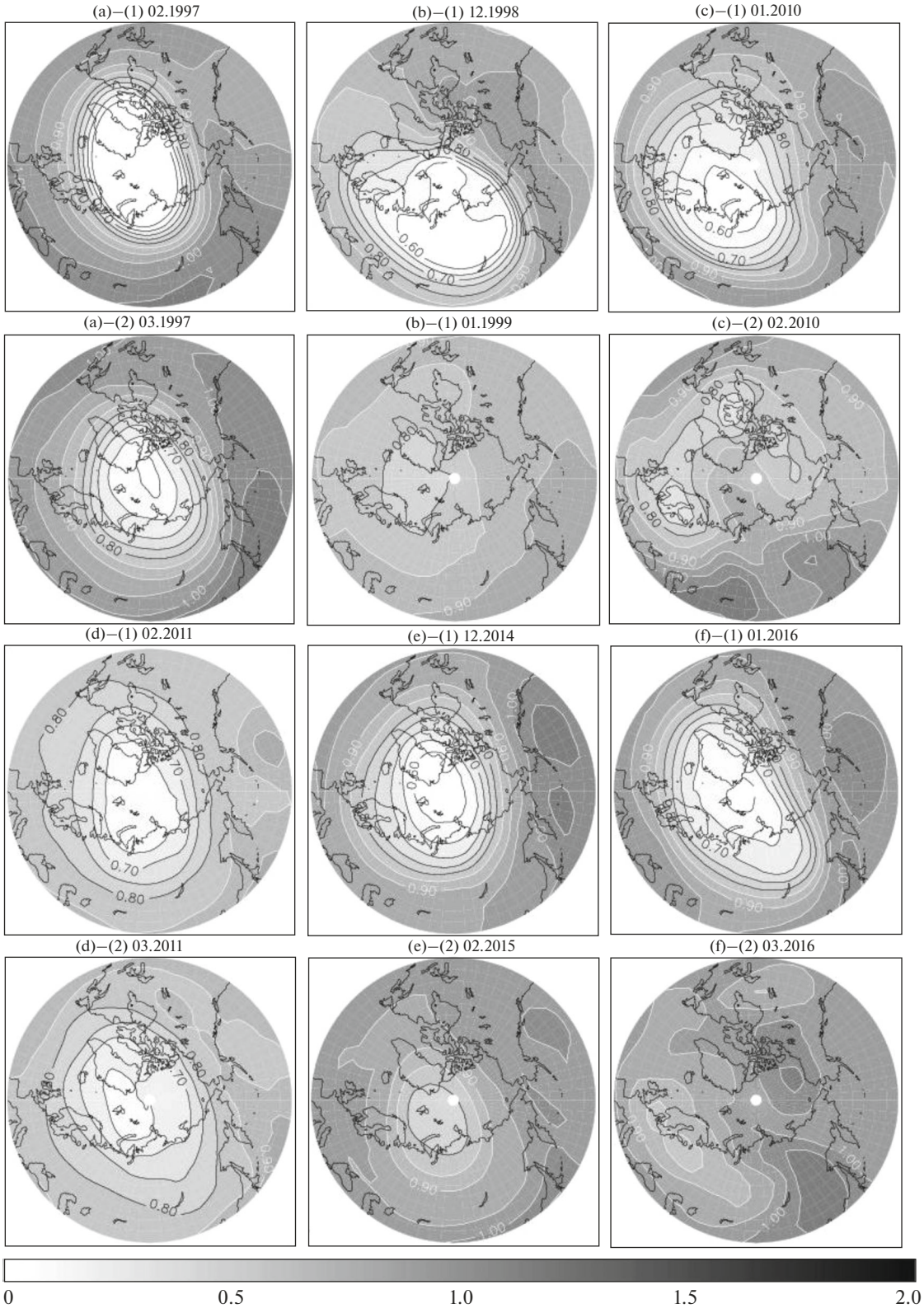

Fig. 6. Monthly mean distribution of the ozone mixing ratio (in $10^5 \frac{\text{kg}}{\text{kg}}$) over the Northern Hemisphere in the 40° N–90° N region at 24.5 km (30 hPa) from ERA-Interim for (column (a)) February and March 1997, (column (b)) December and January 1998–1999, (column (c)) January and February 2010, (column (d)) February and March 2011, (column (e)) December and February 2014–2015, and (column (f)) January and March 2016.

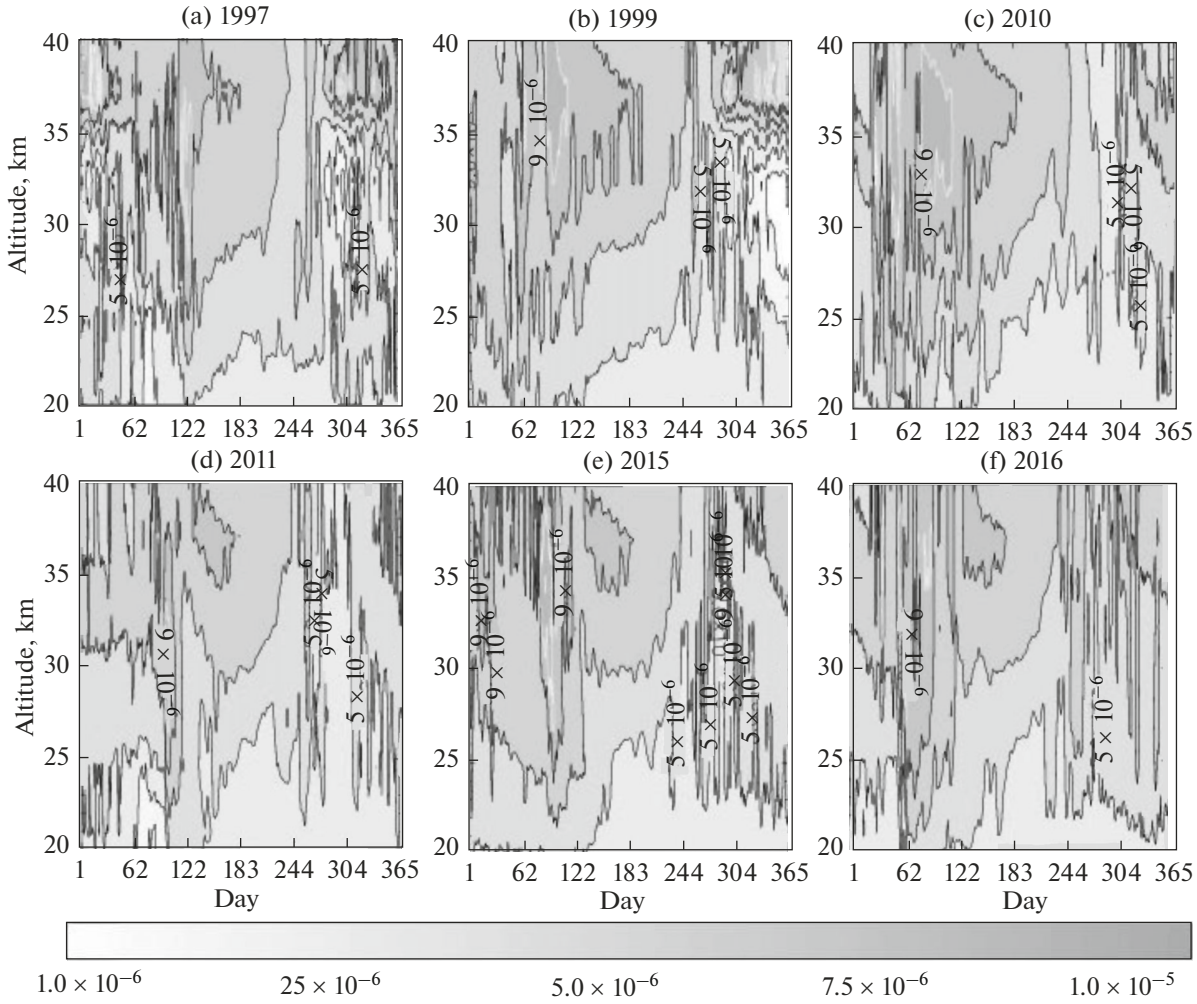

Fig. 7. Vertical annual profiles of the ozone mixing ratio (in $\frac{kg}{kg}$) from the ERA-Interim daily means at 84° N in (a) 1997, (b) 1999, (c) 2010, (d) 2011, (e) 2015, and (f) 2016.

and 2016 (column (f)), a significant decrease in ozone (about 6×10^{-6} $\frac{kg}{kg}$ or 3.6 ppm) was recorded in December and January, but then the amount of ozone began to increase dramatically (up to a mixing ratio of no less than 8×10^{-6} $\frac{kg}{kg}$, or 4.8 ppm), which may have been due to a series of SSWs in those years. In 1999 (column (b)), when the CPV and the low-temperature zone were most unstable, the amount of ozone slightly decreased to a mixing ratio of ~8×10^{-6} $\frac{kg}{kg}$ (4.8 ppm), although there were values of ~$6–7 \times 10^{-6}$ $\frac{kg}{kg}$ (3.6–4.2 ppm) in December 1998 (Fig. 6b–(1)).

The vertical zonal-mean annual profiles of the ozone mixing ratio were also constructed from the ERA-Interim daily means. Profiles for 1997, 1999, 2010, 2011, 2015, and 2016 at 84° N are shown in Figs. 7a–7e.

It is clear from these figures that low ozone mixing ratios ($4–6 \times 10^{-6}$ $\frac{kg}{kg}$, or 2.4–3.6 ppm) were observed at 25–30 km from January to April 1997 (Fig. 7a) and 2011 (Fig. 7d), although values of no less than $6–8 \times 10^{-6}$ $\frac{kg}{kg}$ (3.6–4.8 ppm) were also noted, but a significant decline in ozone occurred in March to April 2011. In 2010 and 2015 (Figs. 7c, 7e), the amount of ozone decreased to $6–8 \times 10^{-6}$ $\frac{kg}{kg}$ (3.6–4.8 ppm) only until February, while in 2016 (Fig. 7f), it decreased until March. In 1999 (Fig. 7b), the ozone mixing ratio at

that time did not drop below $8 \times 10^{-6} \frac{\text{kg}}{\text{kg}}$ (4.8 ppm). In all years, the low amount of ozone with values less than $5 \times 10^{-6} \frac{\text{kg}}{\text{kg}}$ (3.0 ppm) is observed in September–October and less than $3 \times 10^{-6} \frac{\text{kg}}{\text{kg}}$ (1.8 ppm) in December 1999.

The ERA-20C and ERA5 data analysis produces similar results for the ozone mixing ratio. The MERRA analysis shows a steady ozone decline in 1997 until late March, but in other respects the results are close to those of ERA-Interim.

Thus, it can be concluded that the most persistent ozone decline was in 1997, when the CPV and the low-temperature region were most stable. The 2011 ozone decline is less distinct in January and February, but more prominent in March. In 2010, 2015, and 2016, the amount of ozone dropped dramatically in February and March, which may have been caused by a series of SSWs. In 1999, the amount of ozone was hardly reduced at all, which may be due to an unstable CPV. This indicates that El Niño can lead to an ozone increase, because, as was shown above, it can initiate SSWs. Hence, the lack of ozone decline can be indicative of the El Niño effect.

2.5. Total Ozone and Oceanic Impact

Total ozone is defined as being equal to the number of ozone molecules contained in the entire atmospheric column. It also depends on ocean heat fluxes, which can be linked to El Niño and La Niña events with their influence on the general circulation of the atmosphere and on the stability of the circumpolar vortex [15, 26, 27].

Polar projections of Northern Hemisphere total ozone from the ERA-Interim monthly means are shown in Fig. 8. The years are chosen to be the same as those for other data: 1996–1997 and 1998–1999 (columns (a), (b)), 2009–2010 and 2010–2011 (columns (c), (d)), and 2014–2015 and 2015–2016 (columns (e), (f)). The projections of total ozone are given for January and February 2010 and 2015 and for February and March 1997, 1999, 2011, and 2016.

In 1997 and 2011 (columns (a), (d)) over the North Pole, there was a region of the lowest total ozone values (less than 280 DU), which appeared in February–March. This agrees with the existence of the most stable CPV and the most persistent low-temperature zone and with ozone decline in those years. The total ozone around this region is above 400 DU. In 2010 and 2015 (columns (c), (e)), a region with ozone values less than 280 DU existed over the North Pole from December to January, but the amount of ozone increased to 444 DU in February. The situation in 2016 was similar (column (f)), but the total ozone increased only in March (Fig. 8f–(2)). This could be a consequence of a series of SSWs in those years. In 1999 (column (b)), there was a region of higher than normal ozone values over the Arctic (above 444 DU over Scandinavia and up to 460 DU over northern Canada) with no ozone decline, which may have been due to the most unstable CPV in that year.

Thus, it can be concluded that the total column ozone depends on the CPV stability and on the stability of the low-temperature region in the stratosphere. In 1997 and 2011, there was a decline in total ozone in February, while its increase in that month occurred in 2010, 2015, and 2016. High values of total ozone were observed in 1999. Therefore, it can be suggested that El Niño may lead to a series of SSWs and to an increase in total ozone, while La Niña may result in a decrease in total ozone.

CONCLUSIONS

The analysis of the ERA-Interim, MERRA, ERA-20C, and ERA5 air temperature, potential vorticity, ozone mixing ratio, and total ozone datasets over the period from 1980 through 2016 allows the following conclusions:

(1) El Niño events were in 1997, 2010, 2015, and 2016, while La Niña events occurred in 1999 and 2011. The SST was above 27°C across the tropical Pacific in 1997, 2010, 2015, and 2016 and only in its western part in 1999 and 2011.

(2) A stable CPV, as a rule, precedes an El Niño event, and an unstable CPV can be its consequence. The most stable CPV was in 1997, with the 1997–1998 El Niño being one of the strongest events. The CPV in 1999, after this El Niño, was most unstable.

(3) El Niño can initiate SSWs, which lead to the instability of the CPV-related region of low temperature (less than 200 K). In El Niño years (2010, 2015, and 2016) and after El Niño (1999), series of SSWs followed, resulting in the instability of the cold region.

(4) El Niño can lead to an increase in ozone, which is evident in 2010, 2015, and 2016, when the low-ozone region begins to shrink rapidly after February (the ozone mixing ratio increases from 3.6 to 4.8 ppm).

(5) El Niño can lead to an increase in total column ozone over the North Pole, which is evident in 2010, 2015, and 2016 (the total ozone increases from 280 to 420–444 DU during February–March).

Thus, the Southern Oscillation has a global impact on the atmosphere by inducing the instability of the CPV through a greater propagation from the troposphere to the stratosphere of wave activity, which initiates SSWs, and by leading to the filling of the ozone-depleted region and to an increase in total ozone.

The conclusions are based on the reanalysis data covering a period from 1980 through 2016, during which only several strong El Niño–Southern Oscilla-

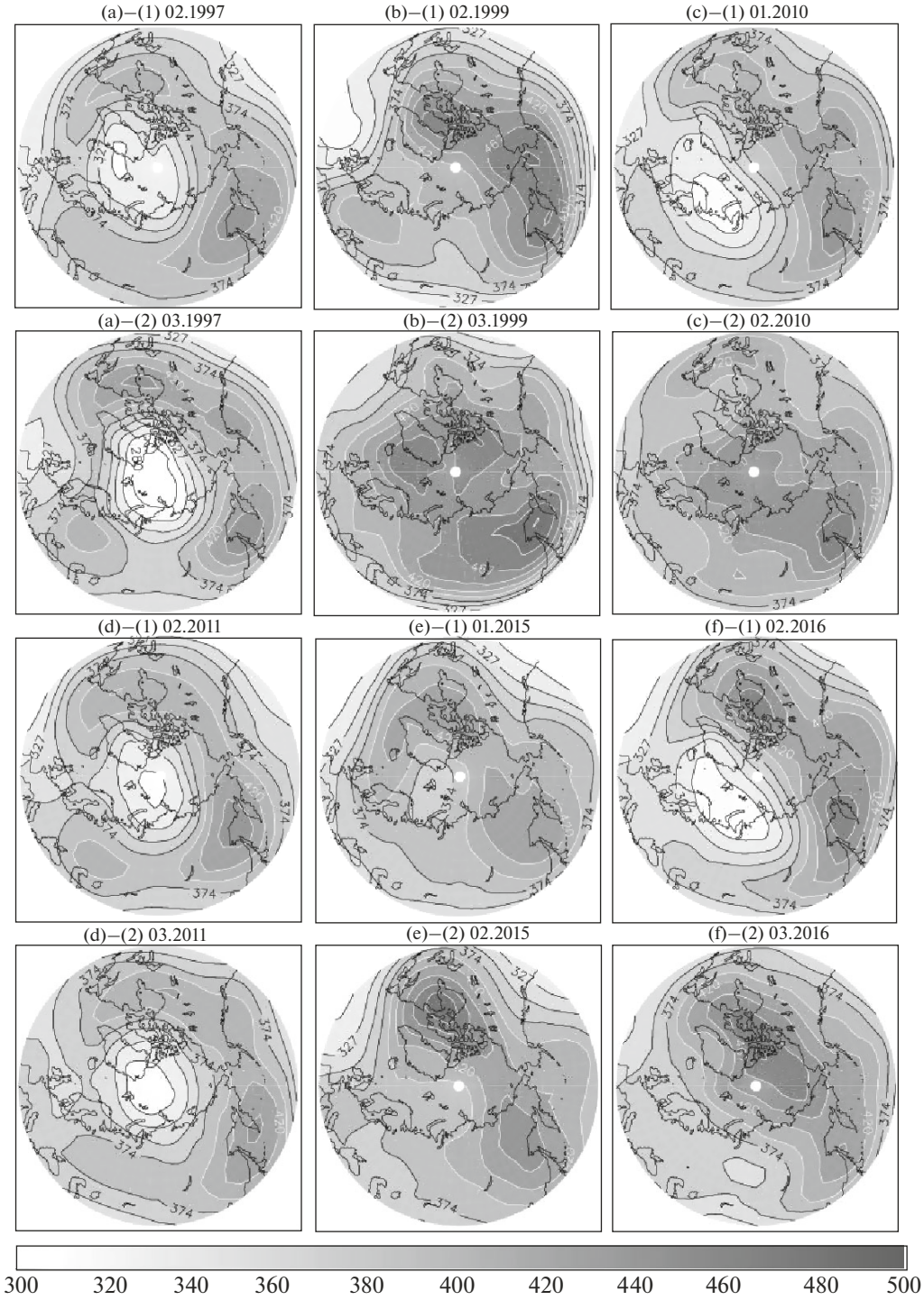

Fig. 8. Monthly mean distribution of total ozone (in Dobson Units) over the Northern Hemisphere at 40° N–90° N from ERA-Interim for February and March (row (a)) 1997 and (row (b)) 1999, (row (c)) January and February 2010, (row (d)) February and March 2011, (row (e)) January and February 2015, and (row (f)) February and March 2016.

tion events occurred. Hence, using climate-modeling data, which have longer time series, as well as the possibility of applying several realizations, for example, for modern climate, can improve and refine the estimates of the atmospheric parameters obtained in the paper.

ACKNOWLEDGMENTS

This work was conducted under project no. 5.6493.2017/8.9 of the governmental task from the Ministry of Science and Higher Education of the Russian Federation. An analysis of the variability of polar

processes was performed under project no. 17-05-01277-a of the Russian Foundation for Basic Research. The assessment of variations in total ozone was performed under project no. 18-05-01050 of the Russian Foundation for Basic Research. We are grateful to an anonymous reviewer for their attention to our paper and helpful remarks.

REFERENCES

1. N. Z. Ariel' and L. A. Strokina, *Dynamical Characteristics of the Atmospheric Interaction with the World Ocean Surface* (Gidrometizdat, Leningrad, 1986) [in Russian].
2. A. B. Bendik and V. N. Yakovlev, "On the convergence of approaches to understanding the El Niño–La Niña phenomenon," Vestn. Ross. Gos. Univ. im. I. Kanta, No. 1, 57–64 (2010).
3. S. S. Lappo, S. K. Gulev, and A. E. Rozhdestvenskii, *Large-Scale Thermal Interaction in the Ocean–Atmosphere System and Energetically Active Regions of the World Ocean* (Gidrometizdat, Leningrad, 1990) [in Russian].
4. A. Czaja, "Ocean–atmosphere coupling in midlatitudes: does it invigorate or damp the storm track?," in *ECMWF Seminar on Seasonal Prediction, 3–7 September 2012* (ECMWF, 2012), pp. 35–46.
5. Yu. P. Doronin, "Ice cover effect on atmosphere–ocean heat exchange," Probl. Arkt. Antarkt., Nos. 43–44, 52–59 (1974).
6. K. E. Taylor, D. Williamson, and F. Zwiers, *The Sea Surface Temperature and Sea-Ice Concentration Boundary Conditions for AMIP II Simulations*, Program for Climate Model Diagnosis and Intercomparison (PCMDI) Rep. No. 60 (University of California, Lawrence Livermore National Laboratory, 2000).
7. K. E. Taylor, D. Williamson, and F. Zwiers, *The Sea Surface Temperature and Sea-Ice Concentration Boundary Conditions for AMIP II Simulations*, Program for Climate Model Diagnosis and Intercomparison (PCMDI) Rep. No. 60 (University of California, Lawrence Livermore National Laboratory, 2000).
8. E. A. Zhadin, "Interannual variations in ozone over Europe and ocean temperature anomalies in the Atlantic," Meteorol. Gidrol., No. 7, 22–26 (1992).
9. E. A. Zhadin, "Long-period cyclicity of ocean surface temperature, lower stratospheric temperature, and ozone at moderate latitudes," Meteorol. Gidrol., No. 5, 52–59 (1993).
10. E. A. Zhadin, "Arctic oscillations and interannual variations in surface temperatures of the Atlantic and Pacific Oceans," Meteorol. Gidrol., No. 8, 28-40 (2001).
11. S. P. Smyshlyaev, A. I. Pogoreltsev, V. Ya. Galin, and E. A. Drobashevskaya, "Influence of wave activity on the composition of the polar stratosphere," Geomagn. Aeron. (Engl. Transl.) **56** (1), 95–109 (2016).
12. P. A. Newman, E. R. Nash, and J. E. Rosenfield, "What controls the temperature of the Arctic stratosphere during the spring?," J. Geophys. Res. **106** (D17), 19999–20010 (2001).
13. D. Hu, W. Tian, F. Xie, J. Shu, and S. Dhomse, "Effects of meridional sea surface temperature changes on stratospheric temperature and circulation," Adv. Atmos. Sci. **31** (4), 888–900 (2014).
14. M. P. Chipperfield and R. L. Jones, "Relative influences of atmospheric chemistry and transport on Arctic ozone trends," Nature **400**, 551–554 (1999).
15. D. Manatsa and G. Mukwada, "A connection from stratospheric ozone to El Niño–Southern Oscillation," Sci. Rep. **7**, 5558 (2017).
16. NASA MERRA. NCAR Climate Data Guide. https://climatedataguide.ucar.edu/climate-data/nasa-merra.
17. ERA-Interim, ECMWF. http://www.ecmwf.int/en/research/climate-reanalysis/era-interim.
18. Weather and Climate Change, Met Office. http://www.metoffice.gov.uk/.
19. V. A. Alekseev, E. M. Volodin, and V. Ya. Galin, Preprint No. 2086-A98, IVM RAN (Institute of Numerical Mathematics, Russian Academy of Sciences, Moscow, 1998).
20. V. Ya. Galin, S. P. Smyshlyaev, and E. M. Volodin, "Combined chemistry–climate model of the atmosphere," Izv., Atmos. Ocean. Phys. **43** (4), 399–412 (2007).
21. A. R. Yakovlev and S. P. Smyshlyaev, "Numerical modeling of the global effect of the ocean and El Niño and La Niña phenomena on the structure and composition of the atmosphere," Uch. Zap. RGGMU, No. 49, 58–72 (2017).
22. Historical El Niño/La Niña episodes (1950–present), United States Climate Prediction Center, 4 November 2015. http://www.cpc.ncep.noaa.gov/products/analysis_monitoring/ensostuff/ensoyears.shtml.
23. P. N. Vargin and E. M. Volodin, "Analysis of the reproduction of dynamic processes in the stratosphere using the climate model of the Institute of Numerical Mathematics, Russian Academy of Sciences," Izv., Atmos. Ocean. Phys. **52** (1), 1–15 (2016).
24. R. Scott and L. Polvani, "Internal variability of the winter stratosphere," J. Atmos. Sci. **63**, 2758–2778 (2006).
25. A. I. Pogoreltsev, E. N. Savenkova, and N. N. Pertsev, "Sudden stratospheric warmings: the role of normal atmospheric modes," Geomagn. Aeron. (Engl. Transl.) **54** (3), 357–372 (2014).
26. A. Karpechko, J. Perlwitz, and E. Manzini, "A model study of tropospheric impacts of the Arctic ozone depletion 2011," J. Geophys. Res. **119** (D13), 7999–8014 (2014).
27. W. T. Ball, J. Alsing, D. J. Mortlock, et al., "Evidence for a continuous decline in lower stratospheric ozone offsetting ozone layer recovery," Atmos. Chem. Phys. **18**, 1379–1394 (2018).
28. C. Bell, L. Gray, A. Charlton-Perez, M. Joshi, A. Scaife, "Stratospheric communication of El Niño teleconnections to European winter," J. Clim. **22**, 4083–4096 (2009).
29. C. Garfinkel and D. Hartmann, "Different ENSO teleconnections and their effects on the stratospheric polar vortex," J. Geophys. Res. **113**, D18114 (2008).
30. A. Butler and L. Polvani, "El Niño, La Niña, and stratospheric sudden warmings: A reevaluation in light of the observational record," Geophys. Res. Lett. **38**, L13807 (2011).

Translated by N. Tret'yakova